SINTECHCOM: Science, Technology and Communication Journal
Vol. 5, No. 3, June 2025, pp. 101-108, DOI: 10.59190/stc.v5i3.310

Design and fabrication of chitin-derived electrodes with optimization of temperature carbonization for energy storage in supercapacitors

Rakhmawati Farma*, Meisya, Irma Apriyani, Awitdrus, Erman Taer
Department of Physics, Universitas Riau, Pekanbaru 28293, Indonesia

ABSTRACT

Supercapacitors have become one of the potential solutions for efficient energy storage, and the development of carbon-based electrodes from biomass has received increasing attention due to their sustainability. This study aims to produce carbon electrodes from crab shells (CS) as biomass materials by optimizing the carbonization process with temperature variations of 600°C, 700°C, and 800°C for supercapacitor cell applications. Material characterization shows that the carbonization temperature of 700°C produces carbon electrodes with optimal semicrystalline structures and mesopore dominance, which supports efficient ion diffusion. The CS-700 carbon electrode showed the highest specific capacitance of 118.84 F/g in cyclic voltammetry tests with 1 M H_2SO_4 electrolyte. These results indicate that carbonization at 700°C provides the best electrochemical performance, making it the optimal condition for developing efficient and environmentally friendly mud crab shell biomass-based electrodes for supercapacitor cell applications.

ARTICLE INFO

Article history:

Received Apr 17, 2025
Revised May 20, 2025
Accepted Jun 24, 2025

Keywords:

Activated Carbon
Carbonization
Chitin
Electrode
Supercapacitor

* **Corresponding Author**
E-mail address: rakhmawati.farma@lecturer.unri.ac.id

1. INTRODUCTION

Energy storage systems have been used for centuries and have experienced continuous improvements due to using renewable energy and the limitations of fossil energy. To overcome these limitations, the development of energy storage devices with high power density, short-term charging-discharging fluctuations, and storing large amounts of energy is one of the right alternatives [1]. Energy storage devices are also important for electrical systems and are classified based on storage period. Short-term energy storage usually involves storing energy for a few hours to a few days, while long-term storage refers to storing energy from a few months to a season (3 – 6 months) [2].

Energy storage types have several categories: electrochemical, thermal, thermochemical, flywheel, compressed-air, pumped storage hydroelectricity, magnetic, chemical, and hydrogen energy storage. Electrochemical energy storage is a device that is being developed and is divided into fuel cells, capacitors, batteries, and supercapacitors [3]. Supercapacitors are high-performance energy storage systems with a storage capacity that can be used when energy sources run low or run out. Supercapacitors are a breakthrough that is still being developed today. Supercapacitors are considered one of the potential devices capable of energy storage due to their high power (charge) storage capacity, long-term cycle stability, flexible operating temperature, and environmentally friendly [4].

The charge storage mechanism or cell configuration in supercapacitors consists of electric double layer capacitors and pseudocapacitors. EDLC supercapacitors consist of electrodes, electrolytes, separators, and current collectors capable of storing energy. These are determined based on the quality of the carbon electrodes. EDLC supercapacitors are generally based on carbon materials, such as activated carbon and graphene dioxide, as active electrode materials because they

have a high surface area and electrical conductivity [5]. Activated carbon has high porosity, a controllable porous structure, chemical stability, and high electrical conductivity. Almost 80% of supercapacitor cells use activated carbon as the electrode material. Activated carbon materials can be produced from various biomass, including red crab shells [6], shrimp shells [7], and fish scales [8]. This study used carbon electrodes based on mangrove crab shell biomass because they are environmentally friendly and inexpensive.

Mangrove crab (*Scylla serrata)* is classified in the Portunidae family, living in almost all coastal waters, especially on mangrove-covered beaches, shallow waters close to mangrove forests, and muddy beaches that play an important role in various ecological functions. Mangrove crab shells can reach around 40% – 60% of the total weight of the crab. The content of mangrove crab shells is chitin ($C_8H_{13}O_5$), protein (COOH-RH-NH_2), and minerals such as magnesium carbonate ($MgCO_3$) and calcium carbonate ($CaCO_3$), so it can potentially be used as a carbon electrode material for supercapacitor cells [9].

This study focuses on manufacturing biomass-based carbon electrodes from crab shells for supercapacitor cell applications by optimizing the carbonization temperature. The carbonization process can decompose chitin, protein, and mineral compounds, which produce activated carbon with a high surface area. The carbonization temperature and activating agent can be one of the factors that affect the pore quality and electrochemical performance of the resulting activated carbon. Previous researchers have used shrimp shell biomass to make carbon electrodes with variations in carbonization temperatures of 700°C, 800°C, and 900°C. The carbonization temperature of 800°C produced the highest specific capacitance value of 303.3 F/g [10]. Researchers Gao et al. (2020) conducted the manufacture of carbon electrodes for supercapacitors with temperature variations of 700°C, 750°C, and 800°C using shrimp shell biomass, which obtained the highest specific capacitance of 201.0 F/g at a temperature of 750°C [11]. Researchers Vinhod et al. (2020) also conducted a study using crab shell biomass for supercapacitor cell electrode applications with carbonization temperature variations of 700°C, 800°C, and 900°C, producing the highest specific capacitance at a temperature of 700°C, namely 266.5 F/g [12]. In this study, the biomass used was crab shells with carbonization temperature variations of 600°C, 700°C, and 800°C.

2. METHODOLOGY

The basic material of crab shells (CS) is collected and cleaned, then dried for 3 days in the sun, which aims to minimise the water content. The next stage is the pre-carbonization process at a temperature of 250℃ for two h. CS is then ground into powder, and carbon is moulded into a coin-shaped solid using a hydraulic press. The carbon in the form of a solid coin is then pyrolyzed. The initial pyrolysis is the carbonization process using N_2 gas with temperature variations of 600°C, 700°C, and 800°C, and the final pyrolysis is the physical activation process using CO_2 gas at a temperature of 900°C. The carbon electrode is neutralised by soaking in distilled water until the pH is neutral.

Structural characterisation of CS was carried out using X-ray diffraction (XRD), Fourier transform infrared (FTIR), and Brunauer-Emmett-Teller (BET) methods. XRD aims to determine the microcrystalline structure using a Panalytical X-Pert Pro PW3060/10 diffractometer with a CuKα light source and using a wavelength of 15.4 nm and a diffraction angle of $2\theta = 10° – 60°$. FTIR testing was carried out using a Shimadzu IR Prestige-21 tool at a wave number of 450 – 4500 nm. Furthermore, BET characterization aims to determine the surface area, diameter, and pore volume of CS. BET testing using Quantachrome Instrument Version 11.0, measuring the amount of gas absorbed by CS at a temperature of 300 °c with a sample mass of ± 0.015 g at 77.3 K.

Supercapacitor cells are made up of several components, namely symmetrical carbon electrodes (CS), current collectors (Stainless steel 316 L), separators (chicken egg shell membranes), and electrolytes (H_2SO_4 1 M). These components are arranged like a sandwich, and electrochemical properties are measured using the cyclic voltammetry (CV) and galvanostatic charge discharge (GCD) methods to analyse the electrochemical behaviour of CS. CV measurement aims to determine the specific capacitance using a symmetrical electrode configuration at a scanning rate of 1, 2, 5, and 10 mV/s and a potential of 0 – 1 V. Furthermore, GCD uses the same configuration at a current density of 1, 2, 5, and 10 A/g and a potential difference of 0 – 1 V.

3. RESULTS AND DISCUSSIONS

Figure 1 shows the XRD pattern of CS, which shows two gentle peaks and several sharp peaks at 2θ angles around 22° – 24° and 42° in the (002) and (100) planes, indicating a semi-crystalline structure.. (Farma, Valensia, et al., 2024). The sharp peaks reflected in Figure 1 indicate the presence of crystalline compounds on the carbon electrode, namely $(C_2F_4)n$, SiO_2, $CaCO_3$, and CaO, which are symbolized by '□', 'Δ', '○', and '◊' respectively. Polytetrafluoroethylene ($(C_2F_4)n$), at an angle of 18.04°, is a compound often found in EDLC supercapacitor cell electrodes, which is interpreted as crystallinity [13]. Silicon dioxide (SiO_2) compounds located at an angle of 26.06°-26.13° are compounds from the basic mineral structure that are not completely decomposed during the manufacture of CS activated carbon. Calcium carbonate ($CaCO_3$) is a mineral that forms CS material at angles of 29.5°, 34.0°, and 39.48°. It shows the decomposition of $CaCO_3$ accompanied by the formation of the CaO phase. Calcium oxide (CaO) is an inorganic crystalline compound in CS that is seen at an angle of 47.15° [14].

The FTIR spectrum of the CS material is shown in Figure 1 (b). At wave numbers 3610.26 and 3629.17 cm^{-1} and 2508.20 cm^{-1}, the presence of hydroxyl (O–H) functional groups was identified, which showed stretching vibrations due to water evaporation or volatile high polarity characteristics [15]. Absorption at 2970.83 cm^{-1} was associated with asymmetric C–H functional groups representing alkyl groups such as methyl and methylene. The presence of this group indicates the occurrence of sp^2 hybridization on several carbon atoms in the amorphous structure. In addition, aromatic compounds were identified at wave numbers 1456.64 cm^{-1}, which are C–C vibrations and are related to the graphitization process, thus potentially increasing the conductivity of carbon. These C–H and C–C functional groups originate from the release of volatile substances during the carbonization process and reflect an increase in carbon content in the material [16]. Meanwhile, the wave number 1736.12–1793.03 cm^{-1} indicates the presence of carbonyl functional groups (C=O), and the range 1033.24–1229.40 cm^{-1} indicates ether functional groups (C–O) [17]. These C=O (anhydride) and C–O (carbonic acid) groups are related to the stretching of oxygen-containing phenol and alcohol groups, which can increase the wettability of the material surface. This increase in wettability contributes to an increase in the specific capacitance value and can affect self-discharge when carbon is used as a supercapacitor electrode [18].

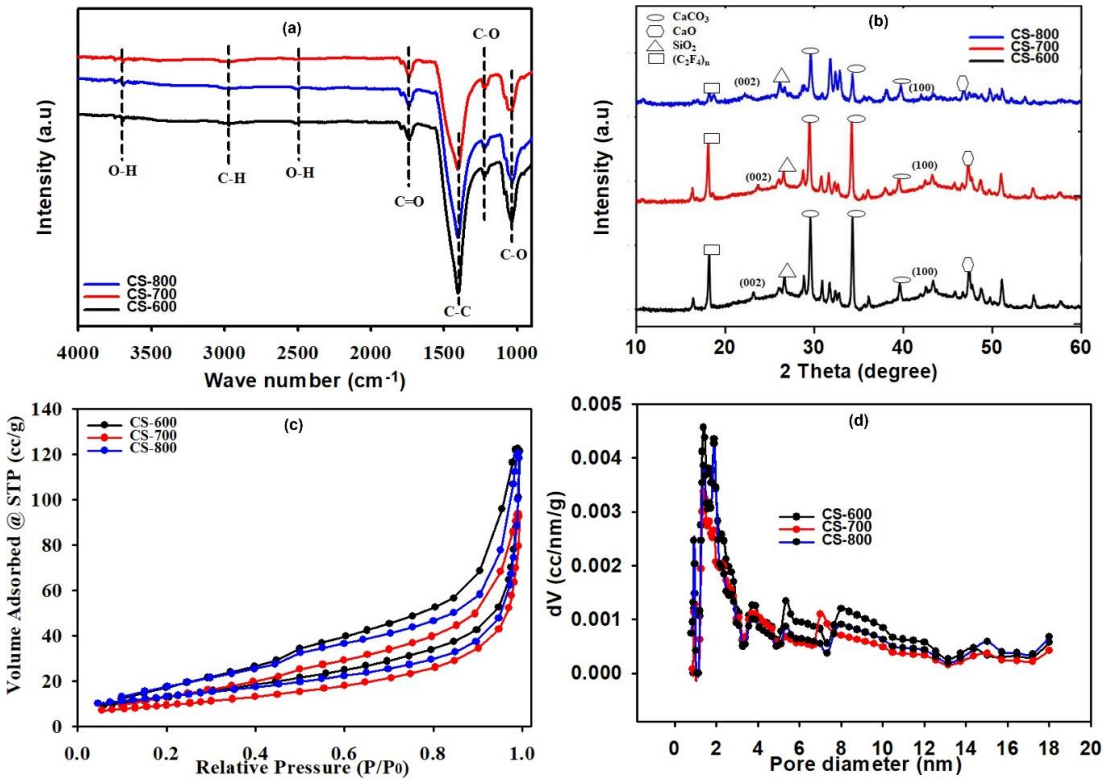

Figure 1. (a) XRD pattern, (b) FTIR spectrum, (c) N_2 adsorption-desorption, (d) pore distribution of CS material.

Table 1 is obtained from data processing using the Bragg and Debye-Scherrer law equations. Increasing the carbonization temperature from 600°C to 700°C can increase the Lc value (graphite plane stack length) because higher thermal energy encourages the improvement of the carbon microstructure through the rearrangement of carbon atoms into more regular graphite stacks. However, the Lc value decreases when the carbonization temperature exceeds 700°C. This is due to further devolatilization and partial gasification processes, such as the formation of CO and CO_2 gases, which produce pores and defects in the carbon structure. In addition, a temperature that is too high can cause local over-graphitization, which results in non-uniformity of the graphite structure and reduces crystal regularity. As a result, although high temperatures initially improve crystallinity, the graphitic structure becomes disrupted at too extreme temperatures, causing a decrease in the L_c value [19].

Table 1. Interlayer spacing and dimensions of the microcrystalline CS.

Sample code	2θ		Interlayer spacing		Dimensions of microcrystalline		Np
	002	100	d_{002} (nm)	d_{100} (nm)	002	100	
CS-600	23.652	42.682	3.759	2.117	9.857	9.926	2.622
CS-700	24.661	42.686	3.607	2.116	23.399	6.540	6.487
CS-800	22.986	42.641	3.886	2.119	7.316	9.048	1.892

Figure 1 (c) shows the isothermal adsorption-desorption curve between relative pressure (P/P_0) and adsorption volume (cm^3/g). Based on the IUPAC classification, this curve shows a significant increase in adsorption on the material surface, indicating the presence of type I and type IV isotherms. At $P/P_0 < 0.2$, an H1 type hysteresis loop is seen, while in the range of $P/P_0 = 0.45 – 0.95$, a wider H4 type hysteresis loop appears, indicating a combination structure between micropores and mesopores [20]. The presence of mesopores, between 2-50 nm in size, is further confirmed through the pore size distribution plot, which shows an average pore radius of 1.5 nm and a dominant pore size of around 15 nm, as shown in Figure 1(d). The significant increase in specific capacitance is associated with increasing mesopores in the carbon electrode structure [21]. Mesopores function as ion reservoirs, which can shorten the ion transport path and accelerate the ion diffusion rate towards the microporous structure. This ultimately increases the electrolyte conductivity and accelerates the charging process in forming an electric double layer capacitor (EDLC) [22].

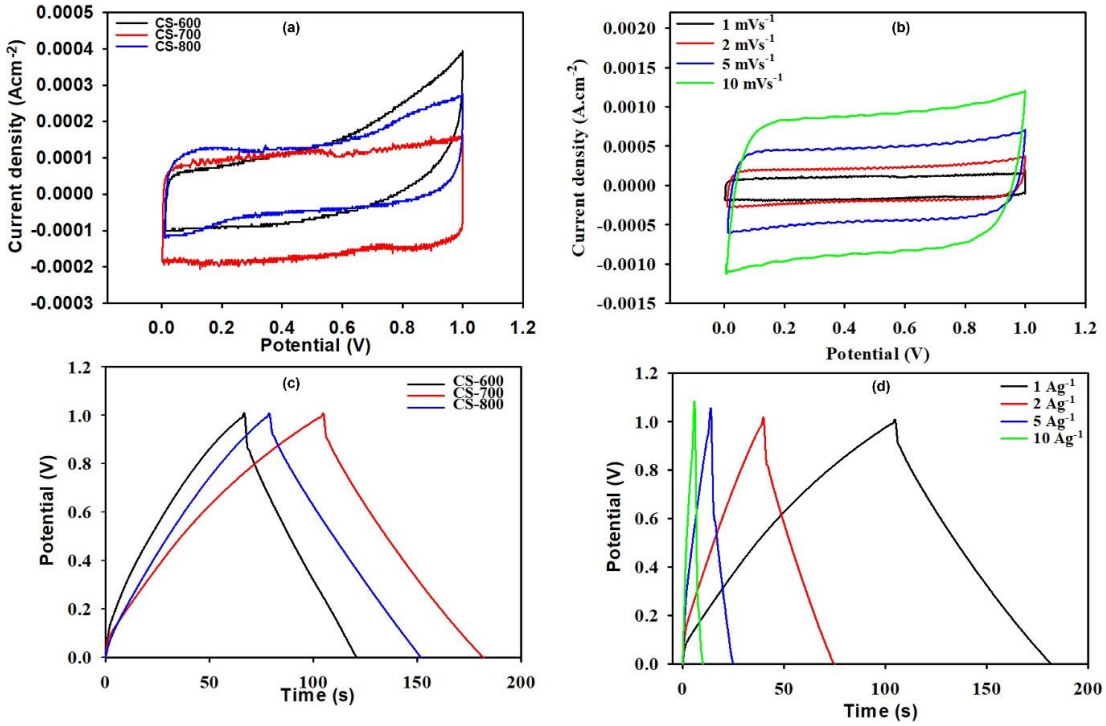

Figure 2. (a) CV curve, (b) CS-700 CV curve, (c) GCD curve, (d) CS-600 GCD curve.

The resulting CV curve shape is quasi-rectangular, a characteristic of an ideal EDLC [23], as shown in Figure 2 (a). CS-700 shows the widest charge-discharge curve area, while CS-600 has the smallest curve area. The greater the charge-discharge current, the wider the resulting curve, which is caused by the increasing number of electrolyte ions participating in the charging and discharging process. This condition results in a higher specific capacitance (Csp).

CS-700 has the highest specific capacitance of 118.84 F/g, while the lowest specific capacitance, with a value of 79.24 F/g, is owned by the CS-600 sample as presented in Table 2. The carbonization temperature of 700°C in the CS-700 sample can produce a large density shrinkage, resulting in high density and multiplying the pore channels, forming many pores. The formation of pores indicates a high capacity to accommodate and absorb anions and cations, increasing the number of ions trapped in the pore channels, which can increase the specific capacitance value of the supercapacitor cell [24].

Table 2. Electrochemical properties test data for supercapacitor cells using the CV method.

Sample code	I_c (A)	I_d (A)	C_{sp} (F/g)	P_{sp} (W/Kg)	E_{sp} (Wh/Kg)
CS-600	0.000128	-0.000070	79.24	39.66	11.01
CS-700	0.000122	-0.000180	118.84	59.48	16.51
CS-800	0.000159	-0.000101	103.96	52.03	14.44

Compared with CS-600 and CS-800 samples, the CS-700 sample showed the best electrochemical performance, characterized by the highest specific capacitance (Csp) value. This achievement is closely related to its optimal physical properties and microstructure. The carbonization temperature of 700°C is considered the best condition in this study because it can optimize the balance between the formation of graphitic structure and the development of porosity. At this temperature, the carbon structure undergoes partial crystallization, which produces an L_c value of 23.399 nm (based on XRD data), indicating an increase in graphite regularity. Based on BET analysis, the formation of abundant mesopores also supports faster ion transport pathways. If the carbonization temperature is too low (as in CS-600), pore formation and crystallization are not optimal, so the structure's regularity decreases. Conversely, temperatures that are too high (as in CS-800) can cause degradation of the micropore and mesopore structures due to shrinkage or sintering. Therefore, 700°C is the optimum temperature for producing carbon electrodes with an ideal combination of graphitic structure regularity and complex pore networks, synergistically enhancing specific capacitance and conductivity stability [25]. In addition, FTIR analysis confirmed the presence of high oxygen (O) content on the surface of carbon electrodes, which plays an important role in increasing surface wettability. This increase in wettability accelerates the diffusion of electrolyte ions, increases self-discharge, and supports the creation of good and stable conductivity [26].

Figure 2 (b), A High scan rate will cause the CV curve to become wider and larger. Increasing the scan rate accelerates the charge and discharge process, which causes the electrolyte ions to move faster towards the electrode. High charge and discharge rates increase the reactivity of the electrode, which can produce a larger current in a shorter time. Conversely, at a low scan rate, the charge-discharge process takes place more slowly, so the resulting curve will be narrower and smaller [27]. A low scan rate gives the electrolyte ions more time to diffuse to the electrode, resulting in a more controlled response and a more compact curve. The asymmetric triangular curve without a significant voltage drop, formed from the relationship between voltage and time at a constant current density of 1 A/g for all samples, shows good EDLC capacitive performance [28], as seen in Figure 2 (c). Charging and discharging on the electrode surface for a longer period (CS-700) results in excellent charge-discharge reversibility, so that the number of electrons and electrolyte ions diffuses maximally, which can increase the specific capacitance of the supercapacitor cell by the CV analysis [29]. Figure 2 (d) shows the GCD curves of CS supercapacitor cells with current densities of 1 , 2, 5, and 10 A/g. The curves maintain an asymmetric quasi-triangular shape even though the current density increases, which is an ideal characteristic of EDLC [30]. At low current densities, the charge-discharge time becomes longer, which results in a larger curve area. This is due to the optimal diffusion of electric charge and electrolyte, which can be well absorbed into the internal pores of the material. On the other

hand, at high current densities, the charge-discharge time becomes shorter, which causes the electric charge and electrolyte not to be optimally absorbed into the material, making the GCD curve smaller.

4. CONCLUSION

This study shows that activated carbon from crab shells, through a carbonization process at a temperature of 700°C, produces carbon electrodes with excellent electrochemical performance. The carbonization temperature of 700°C is the optimal condition that improves the pore structure, with abundant mesopore dominance, and the highest specific capacitance at a value of 118.84 F/g. In addition, the characteristics of the semicrystalline CS material and the presence of functional groups that increase surface wettability support high supercapacitor performance. These results indicate the great potential of using crab shell biomass as an environmentally friendly and efficient raw material for supercapacitor cell electrode applications, and open up opportunities for developing biomass-based carbon materials with more controlled carbonization temperatures.

ACKNOWLEDGEMENTS

The authors are grateful to the Badan Riset dan Inovasi Nasional (BRIN) and Lembaga Pengelola Dana Pendidikan (LPDP), with contract number: 7674/UN19.5.1.3/ AL.04/2023.

REFERENCES

[1] Kumar, K., Tyagi, U., Sirohi, S., Kumar, R., Maity, S. K., Singh, S., & Kumar, G. (2025). A critical review on nanostructure-doped carbonized biomass: A new Era in sustainable supercapacitor technology. *Fuel*, **381**, 133707.

[2] Feng, J., Zhu, Q., Le, Q., Zhu, W., Song, B., Zhang, Z., & Lam, J. C. H. (2025). Source and performance of waste-derived porous carbon material as supercapacitor: Biomass, sludge and plastic waste as precursors. *Renewable and Sustainable Energy Reviews*, **211**, 115178.

[3] Gunasekaran, S. S., Gopalakrishnan, A., Subashchandrabose, R., & Badhulika, S. (2021). Single step, direct pyrolysis assisted synthesis of nitrogen-doped porous carbon nanosheets derived from bamboo wood for high energy density asymmetric supercapacitor. *Journal of Energy Storage*, **42**, 103048.

[4] Liao, H., Zhong, L., Zeng, H., Xiao, Y., Cheng, B., & Lei, S. (2023). A dual-acetate synchronous catalysis-activation strategy towards regulable porous graphitic carbon for high-energy supercapacitor with acetate water-in-salt electrolyte. *Carbon*, **213**, 118305.

[5] Ping, Y., Han, J., Li, J., Xiong, B., Fang, P., & He, C. (2019). N, S co-doped porous carbons from natural Juncus effuses for high performance supercapacitors. *Diamond and Related Materials*, **100**, 107577.

[6] Fu, M., Chen, W., Zhu, X., Yang, B., & Liu, Q. (2019). Crab shell derived multi-hierarchical carbon materials as a typical recycling of waste for high performance supercapacitors. *Carbon*, **141**, 748–757.

[7] Shi, W., Chang, B., Yin, H., Zhang, S., Yang, B., & Dong, X. (2019). Crab shell-derived honeycomb-like graphitized hierarchically porous carbons for satisfactory rate performance of all-solid-state supercapacitors. *Sustainable Energy & Fuels*, **3**(5), 1201–1214.

[8] Paul, A., Chakraborty, A., Samanta, P., Mondal, D., Dhak, D., Murmu, N. C., & Kuila, T. (2023). Bio-waste fish scale: An efficient piezoelectric separator for self-chargeable supercapacitor. *Journal of Energy Storage*, **74**, 109426.

[9] Zhang, H., Sun, X., Zheng, Y., & Zhou, J. (2024). Scalable synthesis of N, O co-doped hierarchical porous carbon for high energy density supercapacitors. *Journal of Colloid and Interface Science*, **658**, 1025–1034.

[10] Wei, X., Qiu, B., Xu, L., Qin, Q., Zhang, W., Liu, Z., Wei, F., & Lv, Y. (2023). High performance hierarchical porous carbon derived from waste shrimp shell for supercapacitor electrodes. *Journal of Energy Storage*, **62**, 106900.

[11] Gao, F., Xie, Y. Q., Zang, Y. H., Zhou, G., Qu, J. Y., & Wu, M. B. (2022). A sustainable strategy to prepare porous carbons with tailored pores from shrimp shell for use as supercapacitor electrode materials. *New Carbon Materials*, **37**(4), 752–763.

[12] Vinodh, R., Sasikumar, Y., Kim, H. J., Atchudan, R., & Yi, M. (2021). Chitin and chitosan based biopolymer derived electrode materials for supercapacitor applications: A critical review. *Journal of Industrial and Engineering Chemistry*, **104**, 155–171.
[13] Sethi, M., Shenoy, U. S., & Bhat, D. K. (2020). A porous graphene–NiFe 2 O 4 nanocomposite with high electrochemical performance and high cycling stability for energy storage applications. *Nanoscale Advances*, **2**(9), 4229–4241.
[14] Borkowski, G., Martyła, A., Dobrosielska, M., Marciniak, P., Gabriel, E., Głowacka, J., Jałbrzykowski, M., Pakuła, D., & Przekop, R. E. (2022). Carbonate lake sediments in the plastics processing-preliminary polylactide composite case study: Mechanical and structural properties. *Materials*, **15**(17), 6106.
[15] Mehdi, R., Naqvi, S. R., Khoja, A. H., & Hussain, R. (2023). Biomass derived activated carbon by chemical surface modification as a source of clean energy for supercapacitor application. *Fuel*, **348,** 128529.
[16] Farma, R., Yunita, A., & Apriyani, I. (2024). Addition of reduced graphene oxide to carbon shaft based on cerbera manghas mesocarp to improve energy storage performance of supercapacitor cells. *Diamond and Related Materials*, **143**, 110922.
[17] Bi, R., Pang, S. K., Yung, K. C., & Yin, L. K. (2022). Comprehensive study of used cigarette filters-derived porous activated carbon for Supercapacitors: From biomass waste to sustainable energy source. *Journal of Electroanalytical Chemistry*, **925**, 116915.
[18] Sesuk, T., Tammawat, P., Jivaganont, P., Somton, K., Limthongkul, P., & Kobsiriphat, W. (2019). Activated carbon derived from coconut coir pith as high performance supercapacitor electrode material. *Journal of Energy Storage*, **25**, 100910.
[19] Farma, R., Refieyana, C., & Apriyani, I. (2024). Biomass valorization of Mangifera Indica into hierarchical carbon materials with self-doping oxygen assisted carbonization for supercapacitor applications. *Energy Sources, Part A: Recovery, Utilization, and Environmental Effects*, **46**(1), 5168-5179.
[20] Yang, Q., Guo, J., Zhang, S., Wang, W., Zhang, X., He, J., & Xu, Y. (2024). Utilizing waste pomelo peel to develop activated-doped porous biomass carbon as electrode materials: Study of activation mechanism, evaluation of electrochemical properties and assembly of symmetric supercapacitors. *Industrial Crops and Products*, **209**, 118060.
[21] Zhang, Y., Zheng, H., Wang, Q., Huang, Y., Li, W., Xiang, J., Huang, W., Yuan, P., Xue, H., Wang, S., Zhou, Y., Lu, W., & Yang, X. (2024). 3-Dimensional porous carbon derived from waste aucklandia lappa straw for high-performance liquid and all-solid-state supercapacitors. *Journal of Electroanalytical Chemistry*, **953**, 117992.
[22] Shaku, B., Mofokeng, T. P., Coville, N. J., Ozoemena, K. I., & Maubane-Nkadimeng, M. S. (2023). Biomass valorisation of marula nutshell waste into nitrogen-doped activated carbon for use in high performance supercapacitors. *Electrochimica Acta*, **442**, 141828.
[23] Apriyani, I., Farma, R., Awitdrus, A., & Yunita, A. (2024). The amorphous porous carbon incorporating 1D-nanofiber as electroactive biomass with integrated pyrolysis for high-performance symmetrical supercapacitors. *Inorganic Chemistry Communications*, **169**, 113069.
[24] Farma, R., Apriyani, I., Deraman, M., Taer, E., Setiadi, R. N., & Rini, A. S. (2023). Enhanced electrochemical performance of oxygen, nitrogen, and sulfur trial-doped Nypa fruticans-based carbon nanofiber for high performance supercapacitors. *Journal of Energy Storage*, **67**, 107611.
[25] Farma, R., Apriyani, I., Awitdrus, A., Taer, E., & Apriwandi, A. (2022). Hemicellulosa-derived Arenga pinnata bunches as free-standing carbon nanofiber membranes for electrode material supercapacitors. *Scientific Reports*, **12**(1), 2572.
[26] Farma, R., Apriyani, I., Zendato, E. R., Awitdrus, A., Setiadi, R. N., & Chitraningrum, N. (2024). Molten salt-confined construction of biocarbon 2D based on Megathyrsus Maximus biomass for high-performance symmetric supercapacitor. *Diamond and Related Materials*, **149**, 111558.
[27] Farma, R., Nur'aini, N. A., Apriyani, I., Awitdrus, A., Taer, E., & Apriwandi, A. (2023). Honeycomb-like carbon with tunable pore size from biomass phoenix dactylifera midrib for highly compressible binder-free supercapacitors. *JOM*, **75**(3), 708–717.

[28] Hsiao, C. H., Gupta, S., Lee, C. Y., & Tai, N. H. (2023). Effects of physical and chemical activations on the performance of biochar applied in supercapacitors. *Applied Surface Science*, **610**, 155560.

[29] Farma, R., Valensia, I., Apriyani, I., Deraman, M., Awitdrus, & Taer, E. (2024). Activated Green Resources from Black Tiger Shrimp Shells to Produce ONP Self-Co-Doped Carbon Nanofiber for High-Performance Supercapacitor. *Journal of Electronic Materials*, **53**(3), 1487–1497.

[30] Mei, Y., Liu, S., Wu, L., Zhou, B., Wang, Z., Huang, Z. H., Zhu, Y., & Wang, M. X. (2024). Kelp derived hierarchically porous carbon aerogels with ultrahigh surface area for high-energy-density supercapacitor in aqueous electrolyte. *Journal of Energy Storage*, **77**, 109878.